

# GMISeg: General Medical Image Segmentation without Re-Training

Jing Xu<sup>1,\*</sup>

1. Department of Computing, Imperial College London, London, UK  
\* j.xu23@imperial.ac.uk

**Abstract:** Although deep learning models have become the main method for medical image segmentation, they often cannot be extended to unknown segmentation tasks involving new anatomical structures, image shapes, or labels. For new segmentation tasks, researchers often have to retrain or fine-tune the model, which is time-consuming and poses a significant obstacle to clinical researchers, who often lack the resources and professional knowledge to train neural networks. Therefore, we proposed a general method that can solve unknown medical image segmentation tasks without requiring additional training. Given an example set of images and prompts for defining new segmentation tasks, GMISeg applies a novel low-rank fine-tuning strategy based on the proposed approach to the SAM (Segment Anything Model) image encoder, and works with the prompt encoder and mask decoder to fine-tune the labeled dataset without the need for additional training. To achieve generalization of new tasks, we used medical image datasets with different imaging modes for different parts. We trained and generalized GMISeg on a different set of anatomical and imaging modes using cardiac images on other site datasets. We have demonstrated that GMISeg outperforms the latest methods on unknown tasks and have conducted a comprehensive analysis and summary of the important performance of the proposed method.

**Keywords:** model generalization, foundation model, low-rank adaptation, medical image segmentation.

## 1 Introduction

Image segmentation is a widely studied issue in computer vision and a core challenge in medical image analysis. Medical segmentation tasks may involve different imaging methods, such as magnetic resonance imaging (MRI), X-ray, computed tomography (CT), and microscopy; Different biomedical fields, such as the abdomen, chest, brain, retina, or individual cells; And different labels within the region, such as the ventricle or epicardium. This diversity inspires a wide range of subdivision models, each typically dealing with a task or a small subset of closely related tasks [1]. In recent years, deep learning models have become the main method for medical image segmentation [2].

A key issue in image segmentation is domain shift, and the model often performs poorly when given examples outside the distribution. This is particularly challenging in the field of medicine, as clinical researchers or other scientists constantly

define new segmentation tasks driven by evolving populations, science, and clinical goals. To address these issues, they need to train the model from scratch or fine-tune the existing model. Unfortunately, training neural networks requires machine learning expertise, computational resources, and manpower. This is not feasible for most clinical researchers or other scientists, as they do not have the professional knowledge or resources to train models. In practice, this greatly slows down the development of science. Therefore, our main research focuses on not conducting any training when given a new segmentation task.

Fine tuning models trained in the field of natural images may not be helpful in the medical field [3], which may be due to differences in data size, features, and task specifications between domains, and importantly, a significant amount of retraining is still needed. Some small semantic segmentation methods attempt to predict new classes in a limited data area without fine-tuning, but mainly focus on classification tasks or segmentation of new classes within the same input domain and cannot generalize across parts or imaging patterns.

In this article, we proposed a generalizable medical image segmentation method that performs well on various tasks without requiring any retraining, including tasks that are fundamentally different from those seen during training. GMISeg learns how to use the input of a set of labeled samples from a specified segmentation task to segment new biomedical images in a forward transfer. We have made the following contributions:

- (1) We proposed GMISeg - a framework that can solve new segmentation tasks without further training: it used a new low-rank fine-tuning strategy, which improves the model's anti-forgetting ability and only adds and updates a small number of parameters during the customization process.
- (2) We have demonstrated that GMISeg performs significantly better than the latest models in segmentation tasks involving different imaging modes of unknown anatomical parts.
- (3) In extensive analysis, we have found that the diversity of tasks during the training process and the size of image capacity during the inference process are related to the generalization ability of the algorithm.

## 2 Related works

**Medical Image Segmentation.** Medical image segmentation has been widely studied, and most methods train convolutional neural networks in a supervised manner to predict label mappings for a given input image [4]. For new segmentation

problems, models are usually trained from scratch and require a lot of design and adjustment.

The latest models, such as nnUNet [5], automate some design decisions, such as data processing or model architecture, but still incur significant consumption due to training. Unlike these methods, GMISeg can be generalized to new medical image segmentation tasks without the need for further training or fine-tuning.

**Multi-task Learning.** Multi-task learning (MTL) framework learns multiple tasks simultaneously [6]. For medical imaging, this may involve multiple forms [7], population centers [8], or anatomical sites [9]. However, tasks are always predetermined by the design: once the training is completed, each network can only solve the tasks proposed during the training process. GMISeg overcomes this limitation by allowing tasks to be dynamically specified during the inference process.

**Transfer Learning.** Transfer learning strategies involve fine-tuning pre-trained models, typically from different fields [10]. This is used for medical image segmentation, starting from models trained on natural images [11], where the amount of data far exceeds that of the target biomedical field. However, this technology still requires extensive training for each new task, which GMISeg avoids. In addition, the differences between medical images and natural images often render transfer learning from large pre-trained models unhelpful [3].

**Optimization-based Meta-Learning.** Optimization-based meta-learning techniques typically learn representations that minimize downstream fine-tuning steps by using several examples for each task, sometimes referred to as less chance learning [12]. Meta-learning through fine-tuning has been studied in medical image segmentation to handle multiple image forms [13], anatomy [14], and generalization of different targets [15]. Although these strategies reduce the amount of data and training required for downstream tasks [16], fine-tuning these models still requires machine learning expertise and computational resources, which are often unavailable to medical researchers.

**Few-shot Semantic Segmentation.** The FS (Few Shot) method typically adapts to new tasks from a few training examples by fine-tuning the pre-trained network [17]. Some few-shot semantic segmentation models generate predictions for new images containing unknown information from only a

few labeled examples without the need for additional retraining. A popular strategy in FS segmentation methods for natural images [18] and medical images [19] is to use large pre-trained models to extract deep features from query and support images. These methods typically involve learning meaningful prototype representations for each label [20]. Another medical FS segmentation strategy uses self-supervised learning to compensate for the shortcomings of training data and tasks [21]. Contrary to GMISeg, these methods focus on limited data strategies, handling specific tasks that involve generalization to new categories in specific subdomains, such as abdominal CT or MRI scans [22, 23] and are only applicable to low dimensional table data. Our solution is based on the ideas of these methods but aims to solve the task of different images to images on a larger scale in multi-anatomical and multimodal medical images.

In our work, we are committed to avoiding any fine-tuning, even when providing many examples for a new task, to avoid requiring clinical or scientific users to have machine learning expertise and computing resources. Our proposed framework aims to extend the model to a wide range of dissections, patterns, and datasets - even those that are completely invisible during training.

### 3 GMISeg Method

Given a medical image  $C$  with a spatial resolution of  $H \times W$  and a channel number of  $x \in R^{H \times W \times C}$ , our goal is to predict its corresponding segmentation image  $\hat{S}$  at the resolution of  $H \times W$ , where each pixel belongs to an element in the predefined category list  $Y = \{y_0, y_1, \dots, y_k\}$ , as close as possible to the real  $S$ . We will use  $y_0$  as the background class and  $y_i, i \in \{1, \dots, k\}$  as the class for different organs. As shown in Figure 1, the overall architecture of GMISeg is inherited from SAM. We froze all parameters in the image encoder and designed a trainable bypass for each transformer block. As shown in Novel LoRA (Novel Low-Rank Adaptation), these bypasses first compress the transformed features into low-level space, and then re-project the compressed features to align with the channels of the output features in the frozen transformer block.

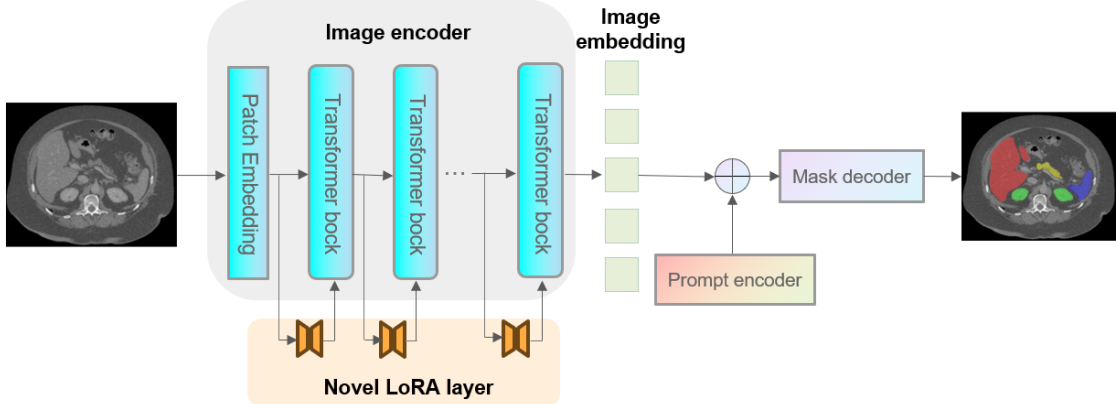


Fig. 1: **The structure of GMISeg.** The framework of GMISeg is consistent with SAM. We froze the image encoder and inserted the proposed trainable Novel LORA layer into SAM for medical image feature extraction.

### 3.1 Novel LoRA in image encoder

The image encoder of GMISeg mainly consists of modules based on ViT (Vision Transformer). However, when fine-tuning a pretrained ViT model for a new task, a key issue is ensuring that the model does not forget its original knowledge. To address this, we proposed a novel approach, applying the LoRA structure to the Q, K, V projection layers of ViT, further enhancing its expressiveness and robustness.

In the standard ViT framework, Q, K, V stand for Query, Key, and Value respectively, which form the core components of the self-attention mechanism in Transformers. As illustrated in Figure 2, we introduced LoRA layers to Q and V, enabling them to undergo parameter updates more efficiently while retaining

the original knowledge. Specifically, this design allows the model to update only a small portion of its parameters during fine-tuning rather than fully retraining the entire model.

The essence of LoRA is low-rank approximation, which can be viewed as a specific parameterization method capable of approximating a large transformation matrix with a limited number of parameters. The motivation for this design is that when fine-tuning a model, task-related information often resides in a low-dimensional subspace rather than being scattered across the entire parameter space. Hence, with LoRA, we can solely update this low-dimensional subspace, leading to more efficient fine-tuning.

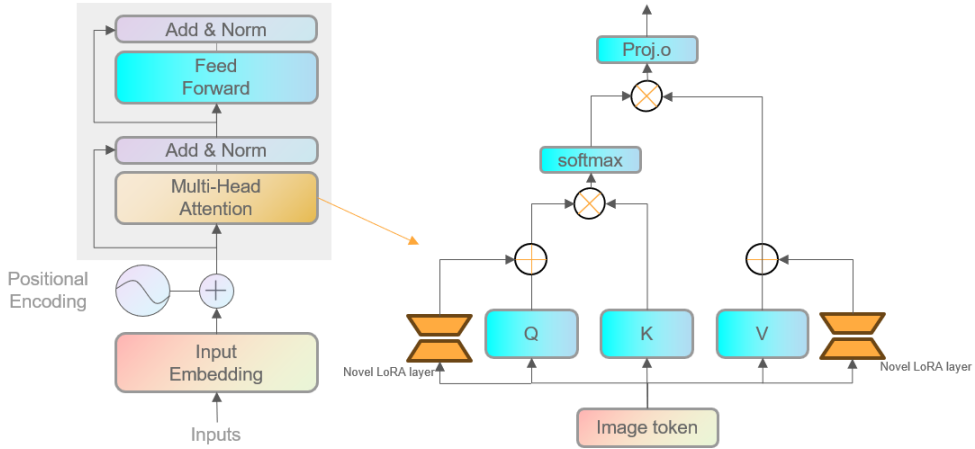


Fig. 2: **The structure of Novel LoRA in image encoder.** We apply the Novel LoRA layer to the q and v projection layers of each transform block in the image encoder. 'Q', 'K', 'V', and 'Proj. o' represent the projection layers of q, k, v, and o.

Equation (1) described how the weight matrix  $W$  is updated, where  $A$  and  $B$  are two linear layers,  $\Delta W$  is the cumulative gradient update during the adaptation process, and  $F$  is the sequences of tokens.

In our design, LoRA not only encompasses the MLP structure of the encoder and decoder but also integrates an average pooling structure. The inclusion of average pooling enhances the rigidity of the model, allowing it to better retain original knowledge. Simultaneously, it boosts the plasticity of the model, enabling it to adapt better to new tasks.

Equation (2) illustrates how  $Q$ ,  $K$ ,  $V$  are processed, where  $W_q$  and  $W_k$  are pretrained projection layers, and  $A_q$  and  $B_q$  are trainable LoRA parameters,  $T$  is the transformer's multi headed attention,  $C_{out}$  is variance.

$$tt(Q, K, V) = \text{Softmax} \left( \frac{Q^T K}{\sqrt{C_{out}}} + B \right) V$$

$$Q = \widehat{W}_q F = W_q F + B_q A_q F$$

$$K = W_k F$$
(2)

$$\widehat{F} = WF$$

$$\widehat{W} = W + \Delta W = W + BA$$
(1)

### 3.2 Novel LoRA embedding

Usually, the incorporated LoRA layer is the MLP structure of the encoder and decoder, but there is a problem with this structure, which will cause catastrophic forgetting of the large model, that is, when the medical data set is used to adjust, the model will forget the pre-trained knowledge. Therefore, this study incorporates the loose LoRA layer, that is, each MLP (each layer of MLP, including the encoder and decoder) is transformed into a vector of the same size through an average pooling operation. This structure is loose enough to improve the rigidity (anti-forgetting ability) and plasticity (learning ability and generalization ability) of the model.

From Figure 3, we can see that the Novel LoRA contains two parts, encoder and decoder. We extract AVG pooling from each layer of encoder and decoder, and concatenate them to form a large matrix, which replaces the original LoRA layer.

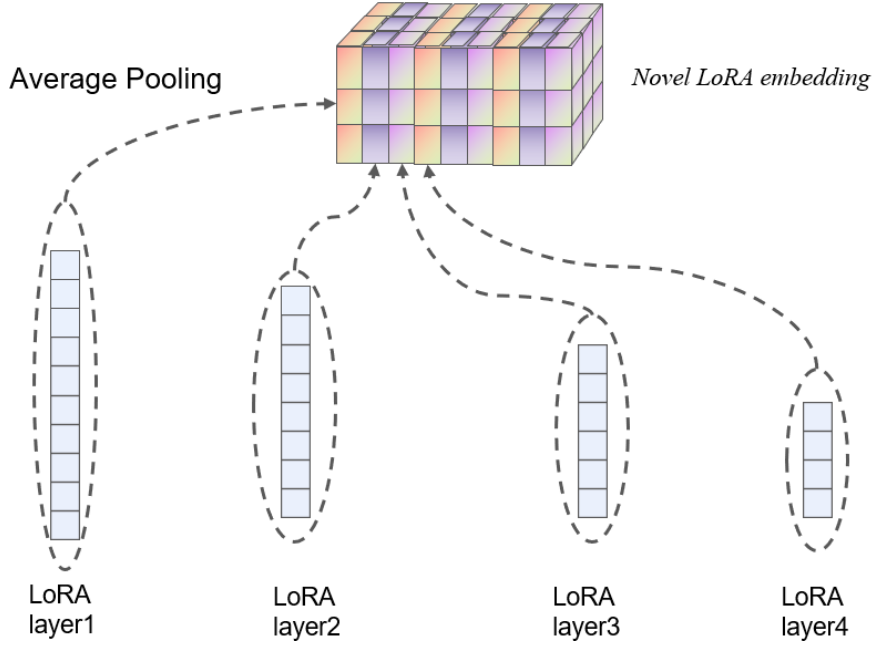


Fig. 3: **The structure of Novel LoRA embedding.** New LoRA converts each MLP (each layer of MLP, including encoder and decoder) into a vector of the same size through an average pooling operation.

### 3.3 Training strategies

**Loss function.** GMISeg uses focal loss and dice loss to monitor the fine-tuning process. The loss function can be described as:

$$L = \mu_1 \text{Focal}(\hat{S}_l, D(S)) + \mu_2 \text{Dice}(\hat{S}_l, D(S)) \quad (3)$$

Where *Focal* and *Dice* denote focal loss and dice loss, respectively.  $D$  represents the downsampling operation so that the resolution of ground truth is the same as that of GMISeg's output because its spatial resolution is much lower.  $\mu_1$  and  $\mu_2$  represent the loss of weight to balance the impact between these two loss items.

**Prompt encoder generation.** Randomly select one or more points in *GroundTruth* to form a set of points, and select the maximum edge in *GroundTruth* to add an offset to generate a box, thus simulating user input.

## 4 Experiments

We begin by describing the dataset and implementation details. The first group of experiments compared the performance of GMISeg in all datasets with the latest generalized medical image segmentation methods. Then, we reported various analyses, including the impact of training task diversity, support set size, and the number of available examples for new tasks.

### 4.1 Datasets

To train and test our general model, we adopt a set of large and diverse segmentation tasks in order to extend it to new tasks. The widely open medical segmentation datasets we used have different anatomic structures, imaging methods, and labels. The training set contains only the cardiac image. The testing set

consists of 5 datasets, covering 4 medical fields and 3 imaging modes.

We standardized the data in various formats of the original dataset, processed images, and label maps. We also use synthetic segmentation tasks to expand the training data to further increase the diversity of training tasks.

The dataset has a wide range of biomedical fields, such as the cardiac (ACDC [24], MICCAI 2018 [25]), abdomen (Synapses [1]), brain (ISLES 2022 [27]), and retina (STARE [26]). A detailed list of datasets is provided in Table 1. Although the dataset has various imaging tasks and labeling protocols, in this work, we focus on the general problem of 2D binary segmentation. For datasets with 3D data, for each object, we extracted the 2D middle layer of the volume along all principal axes.

**Table 1: Test dataset.**

Dataset Name	Description	# of Scans	Image Modalities
ACDC	Left and right ventricular endocardium	99	cine-MRI
MICCAI 2018	Left atria	100	MRI
Synapses	Abdominal organs	3779	CT
STARE	Blood vessels in retinal images	20	Optical camera
ISLES 2022	Ischemic stroke lesion	180	multi-modal MRI

## 4.2 Implementation details

We adopted the data enhancement strategy of random flip and random Gaussian noise and carried out all experiments based on the "vit\_L" version of SAM. We first upsampled all images to  $1024 \times 1024$ , and then input the up-sampled image into GMISeg to maintain a better image resolution of the predicted segmentation Logit. The new LoRA is used to fine-tune the frozen  $Q$  and  $V$  projection layers of the transformer block. For efficiency and performance optimization, the grade of LoRA was set to 4. The weight of focal loss set is 1, and the weight of dice loss set is 1.

Table 2: **Performance summary.** We report the average dice score, Jaccard score, and ASD values for each dataset of each model.

Method	Dataset	Dice (%)	Jaccard (%)	ASD (mm)
<b>Our Method</b>	ACDC	<b>78.7</b>	<b>74.5</b>	<b>1.2</b>
CycleGAN	ACDC	75.5	72.1	2.4
UniverSeg	ACDC	75.0	71.6	2.7
Neuralizer	ACDC	74.7	71.2	3.1
<b>Our Method</b>	MICCAI 2018	<b>77.8</b>	<b>84.3</b>	<b>1.3</b>
CycleGAN	MICCAI 2018	75.3	71.9	2.5
UniverSeg	MICCAI 2018	74.9	71.4	2.8
Neuralizer	MICCAI 2018	74.5	71.0	3.3
<b>Our Method</b>	Synapses	<b>77.5</b>	<b>73.9</b>	<b>1.4</b>
CycleGAN	Synapses	75.0	71.5	2.6
UniverSeg	Synapses	74.6	71.1	3.0
Neuralizer	Synapses	74.2	70.8	3.4
<b>Our Method</b>	STARE	<b>77.6</b>	<b>74.0</b>	<b>1.5</b>
CycleGAN	STARE	74.9	71.3	2.9
UniverSeg	STARE	74.4	70.9	3.2
Neuralizer	STARE	74.0	70.5	3.6
<b>Our Method</b>	ISLES 2022	<b>78.3</b>	<b>76.3</b>	<b>1.6</b>
CycleGAN	ISLES 2022	74.3	69.9	3.6
UniverSeg	ISLES 2022	74.9	73.2	3.0
Neuralizer	ISLES 2022	74.5	72.8	2.9

## 4.3 Task Generalization Results

We compared the segmentation performance of GMISeg with the latest generalized segmentation models CycleGAN, Neuralizer, and Uniferseg. Our main objective was to evaluate the effectiveness of GMISeg in solving tasks from unknown datasets. Table 2 shows the average Dice score, Jaccard score, and ASD values of each dataset for each method, and Figure 4 shows an example of segmentation visualization results for each dataset of each method.

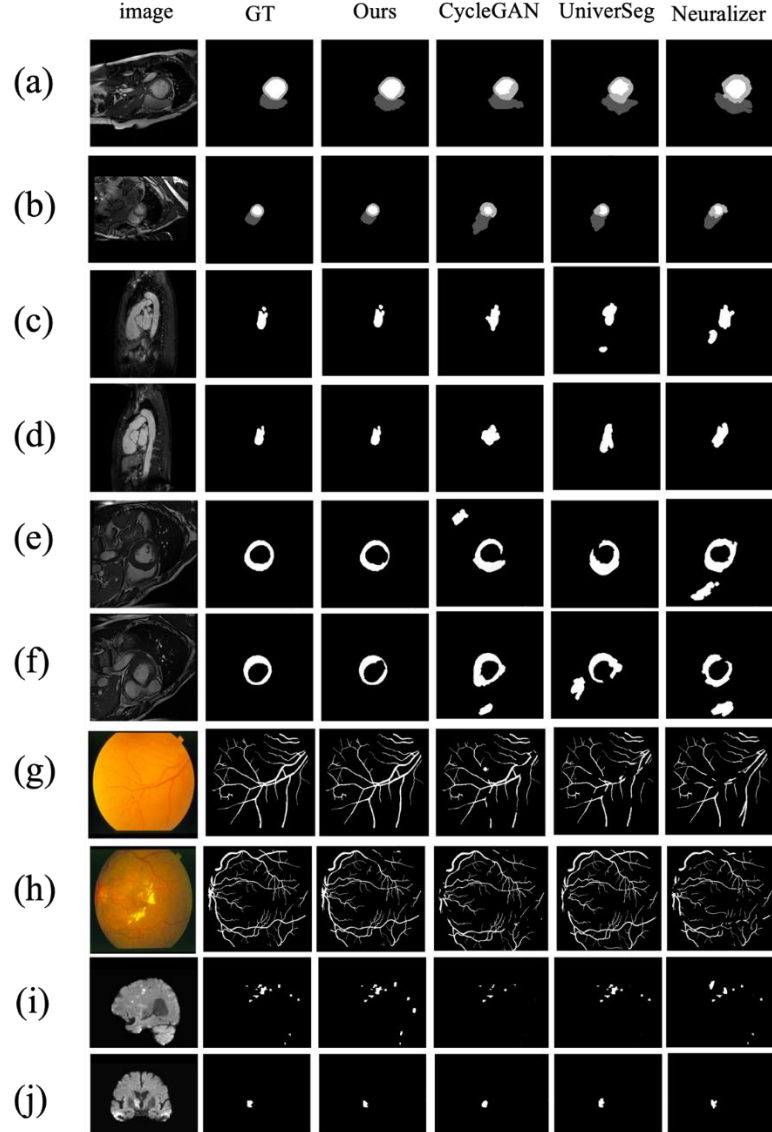


Fig. 4: **Example model predictions for unseen tasks.** For randomly sampled images of each segmentation task, we visualized the predictions of GMISeg and the three latest models, as well as GroundTruth maps. Among them, (a) (b) comes from ACDC, (c) (d) comes from MICCAI 2018, (e) (f) comes from Synapse, (g) (h) comes from STARE, and (i) (j) comes from ISLES 2022.

Table 2 shows that in all datasets, GMISeg's performance is significantly better than all the latest methods, with Dice's improvement range from 3.2% to 4.0%, Jaccard's improvement range from 2.4% to 13.3%, and ASD's improvement range from 1.2mm to 2.1mm.

Figure 4 also shows the obvious quality improvement in generalization segmentation. Compared with other methods, the segmented region predicted by GMISeg is smoother and more accurate. We attribute this phenomenon to the powerful feature extraction ability of large-scale SAM models and the effective fine-tuning strategy adopted by GMISeg.

#### 4.4 Analysis

**Task Quantity and Diversity.** We investigated the number of datasets used to train GMISeg and the impact of individual tasks. We omitted the synthesis task in this experiment and trained the model on a random subset of the training dataset.

Figure 5 shows the performance of different random subsets of the training dataset on the test dataset. We found that the more training tasks, the better performance on test tasks. In some cases, the selection of datasets can have a great impact. For example, for a model trained with a 10% dataset, the best model has a Dice score nearly 23% higher than the worst model.

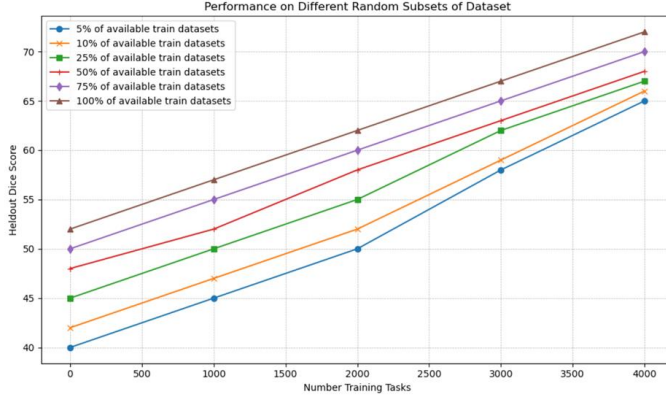


Fig. 5: Average Dice versus the number of training tasks points represent individual networks trained according to the percentage of available training datasets and are displayed by the number of basic training tasks.

**Support Set Size.** We explored the effect of support size on the training model with support  $N$  ranging from 1 to 64.

Figure 6 shows that the best results are obtained with a larger training support size, and the average Dice score rapidly

increases from 57.6% to 69.1% with support sizes ranging from 1 to 64. We found that ensemble prediction leads to improvement in support size ( $N > 6$ ).

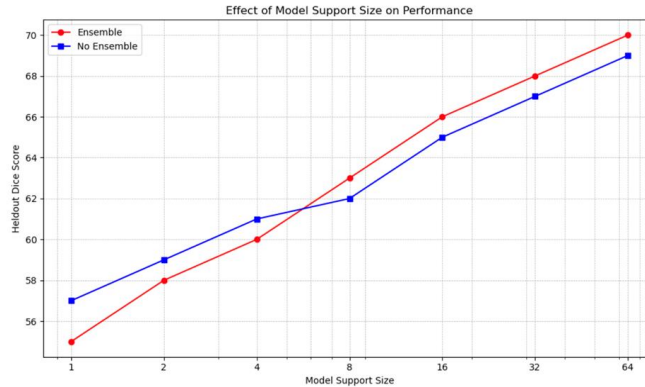


Fig. 6: Effects of support size the relationship between the models trained at a specific support set size and their dice average scores. With the increase in support size, the results will be improved, and the integration will always help.

**Limited Example Data.** Since manually annotating examples in new tasks is costly for medical dataset, we investigated how the number of labeled images affects the performance of GMISeg. We used a limited number of labeled

examples  $n$  to study GMISeg when reasoning, where  $n = 1, 2, 64$ . we performed 100 replicates for each size, each corresponding to an independent random subset of the data. Here, the support set contains all data available for reasoning, so we do not perform integration.

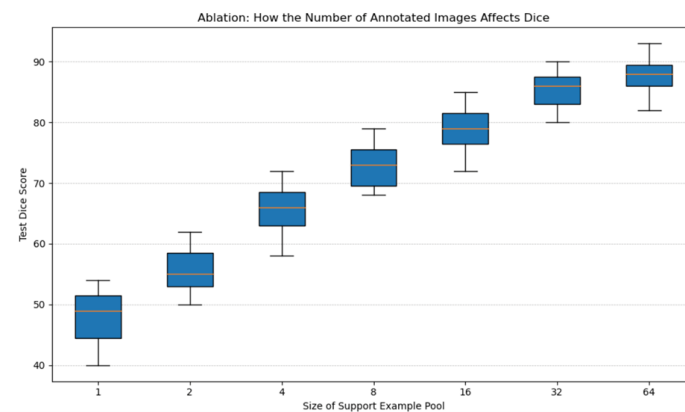


Fig. 7: Effect of available data at influence GMISeg predictions using limited data samples on the supporting STARE dataset. For each size, we performed 100 replicates using different random subsets.

Figure 7 shows the results of the STARE dataset. For the smaller support size  $n$ , we observed a huge difference caused by the very diverse support set. As  $n$  increases, we observe that

## 5 Conclusion

We introduce GMISeg, a single-task agnostic model for learning medical image segmentation. We used a large number of diverse open-access medical segmentation datasets to train and test GMISeg, which can be generalized to unknown anatomy and tasks. We proposed a novel low-rank fine-tuning strategy, which improves the anti-forgetting ability of the model by extracting and merging the loose layer structure, and it can only add and update a small number of parameters in the customization process, thus improving the learning ability and generalization ability of model.

In our experiment, the results of GMISeg on all datasets are much better than the latest generalized medical image segmentation methods. Through extensive in-depth research, we concluded that the performance of GMISeg strongly depends on task diversity during training and the size of the support set during reasoning.

In this work, we used 2D data and a single tag to highlight and analyzed the core functions of GMISeg. In the future, we plan to use 2.5D or 3D models and multi-label map segmentation 3D volume to expand the model. GMISeg is expected to successfully adapt to the new segmentation tasks determined by scientists and clinical researchers without the need for model retraining which is usually impractical for them.

## Acknowledgement

We thank NVIDIA Corporation for the GPU donation.

## Data availability

The data are available upon request.

## Declaration of Conflicts of Interest

The authors declare that there are no conflicts of interest in this study.

## References

[1] J. Chen, Y. Lu, Q. Yu, et al. Transunet: Transformers make strong encoders for medical image segmentation[J]. *arXiv preprint arXiv:2102.04306*, 2021.

[2] F. Milletari, N. Navab, S. A. Ahmadi. V-net: Fully convolutional neural networks for volumetric medical image segmentation[C]//2016 fourth international conference on 3D vision (3DV). Ieee, 2016: 565-571.

[3] M. Raghu, C. Zhang, J. Kleinberg, et al. Transfusion: Understanding transfer learning for medical imaging[J]. *Advances in neural information processing systems*, 2019, 32.

[4] J. Dolz, K. Gopinath, J. Yuan, et al. HyperDense-Net: a hyper-densely connected CNN for multi-modal image segmentation[J]. *IEEE transactions on medical imaging*, 2018, 38(5): 1116-1126.

[5] F. Isensee, P. F. Jaeger, S. A. A. Kohl, et al. nnU-Net: a self-configuring method for deep learning-based biomedical image segmentation[J]. *Nature methods*, 2021, 18(2): 203-211.

[6] R. Caruana. Multitask learning[J]. *Machine learning*, 1997, 28: 41-75.

[7] P. Moeskops, J. M. Wolterink, B. H. M. Van Der Velden, et al. Deep learning for multi-task medical image segmentation in multiple modalities[C]//*Medical Image Computing and Computer-Assisted Intervention–MICCAI* 2016: 19th International Conference, Athens, Greece, October 17-21, 2016, Proceedings, Part II 19. Springer International Publishing, 2016: 478-486.

[8] Q. Liu, Q. Dou, L. Yu, et al. MS-Net: multi-site network for improving prostate segmentation with heterogeneous MRI data[J]. *IEEE transactions on medical imaging*, 2020, 39(9): 2713-2724.

[9] F. Navarro, S. Shit, I. Ezhov, et al. Shape-aware complementary-task learning for multi-organ segmentation[C]//*Machine Learning in Medical Imaging: 10th International Workshop*, MLMI 2019, Held in Conjunction with MICCAI 2019, Shenzhen, China, October 13, 2019, Proceedings 10. Springer International Publishing, 2019: 620-627.

[10] J. M. J. Valanarasu, P. Oza, I. Hacihamoglu, et al. Medica Sun B, Feng J, Saenko K. Return of frustratingly easy domain adaptation[C]//*Proceedings of the AAAI conference on artificial intelligence*. 2016, 30(1).

[11] Z. Zhou, V. Sodha, J. Pang, et al. Models genesis[J]. *Medical image analysis*, 2021, 67: 101840.

[12] C. Finn, P. Abbeel, S. Levine. Model-agnostic meta-learning for fast adaptation of deep networks[C]//*International conference on machine learning*. PMLR, 2017: 1126-1135.

[13] Y. Zhang, J. Yang, J. Tian, et al. Modality-aware mutual learning for multi-modal medical image segmentation[C]//*Medical Image Computing and Computer Assisted Intervention–MICCAI* 2021: 24th International Conference, Strasbourg, France, September 27–October 1, 2021, Proceedings, Part I 24. Springer International Publishing, 2021: 589-599.

[14] P. Zhang, J. Li, Y. Wang, et al. Domain adaptation for medical image segmentation: A meta-learning method[J]. *Journal of Imaging*, 2021, 7(2): 31.

[15] R. Khadka, D. Jha, S. Hicks, et al. Meta-learning with implicit gradients in a few-shot setting for medical image segmentation[J]. *Computers in Biology and Medicine*, 2022, 143: 105227.

[16] K. He, R. Girshick, P. Dollár. Rethinking imagenet pre-training[C]//*Proceedings of the IEEE/CVF International Conference on Computer Vision*. 2019: 4918-4927.

[17] U. Baid, S. Ghodasara, S. Mohan, et al. The rsna-asnr-miccai brats 2021 benchmark on brain tumor segmentation and radiogenomic classification[J]. *arXiv preprint arXiv:2107.02314*, 2021.

the average segmentation quality monotonically improves and the variance with the sample of available data greatly decreases.

[18] J. Seo, Y. H. Park , S. W. Yoon, et al. Task-Adaptive Feature Transformer with Semantic Enrichment for Few-Shot Segmentation[J]. *arXiv preprint arXiv:2202.06498*, 2022.

[19] H. Ding, C. Sun, H. Tang, et al. Few-shot medical image segmentation with cycle-resemblance attention[C]//*Proceedings of the IEEE/CVF Winter Conference on Applications of Computer Vision*. 2023: 2488-2497.

[20] K. Wang, J. H. Liew, Y. Zou, et al. Panet: Few-shot image semantic segmentation with prototype alignment[C]//*proceedings of the IEEE/CVF international conference on computer vision*. 2019: 9197-9206.

[21] S. Hansen, S. Gautam, R. Jenssen, et al. Anomaly detection-inspired few-shot medical image segmentation through self-supervision with supervoxels[J]. *Medical Image Analysis*, 2022, 78: 102385.

[22] A. G. Roy, S. Siddiqui, S. Pölsterl, et al. ‘Squeeze & excite’-guided few-shot segmentation of volumetric images[J]. *Medical image analysis*, 2020, 59: 101587.

[23] H. Tang, X. Liu, S. Sun, et al. Recurrent mask refinement for few-shot medical image segmentation[C]//*Proceedings of the IEEE/CVF international conference on computer vision*. 2021: 3918-3928.

[24] O. Bernard, A. Lalande, C. Zotti, et al. Deep learning techniques for automatic MRI cardiac multi-structures segmentation and diagnosis: is the problem solved?[J]. *IEEE transactions on medical imaging*, 2018, 37(11): 2514-2525.

[25] Z. Xiong, Q. Xia, Z. Hu, et al. A global benchmark of algorithms for segmenting the left atrium from late gadolinium-enhanced cardiac magnetic resonance imaging[J]. *Medical image analysis*, 2021, 67: 101832.

[26] A. D. Hoover, V. Kouznetsova, M. Goldbaum. Locating blood vessels in retinal images by piecewise threshold probing of a matched filter response[J]. *IEEE Transactions on Medical imaging*, 2000, 19(3): 203-210.

[27] M. R. Hernandez Petzsche, E. de la Rosa, U. Hanning, et al. ISLES 2022: A multi-center magnetic resonance imaging stroke lesion segmentation dataset[J]. *Scientific data*, 2022, 9(1): 762.